Supporting Information

MANUSCRIPT TITLE: Redox Behavior of Uranium at the Nanoporous Aluminum Oxide-Water Interface: Implication for Uranium Remediation

AUTHOR NAMES: Hun Bok Jung[1,#], Maxim I. Boyanov[2], Hiromi Konishi[1], Yubing Sun[1], Bhoopesh Mishra[2], Kenneth M. Kemner[2], Eric Roden[1], and Huifang Xu[*, 1]

AUTHOR ADDRESSES:

1. University of Wisconsin, Department of Geoscience Madison, WI 53706 USA
2. Biosciences Division, Argonne National Laboratory, Argonne, IL 60439 USA

Present address for Hun Bok Jung: Pacific Northwest National Laboratory, Richland WA 99354, USA

NUMBER OF PAGES: 14

NUMBER OF TABLES: 2

NUMBER OF FIGURES: 9

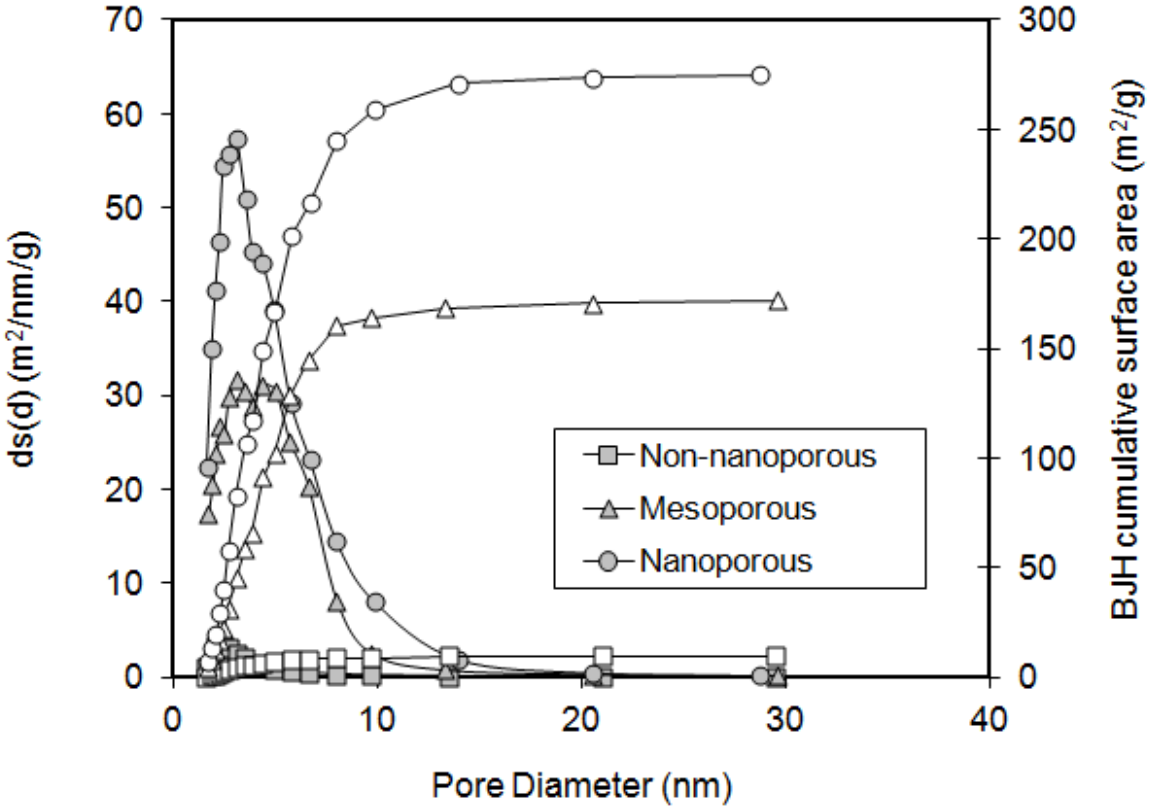

Fig. S1. Pore size and surface area analysis for 3 types of aluminum oxides. The lines with open symbols indicate BJH cumulative surface area, while the lines with gray colored symbols show dS(d).

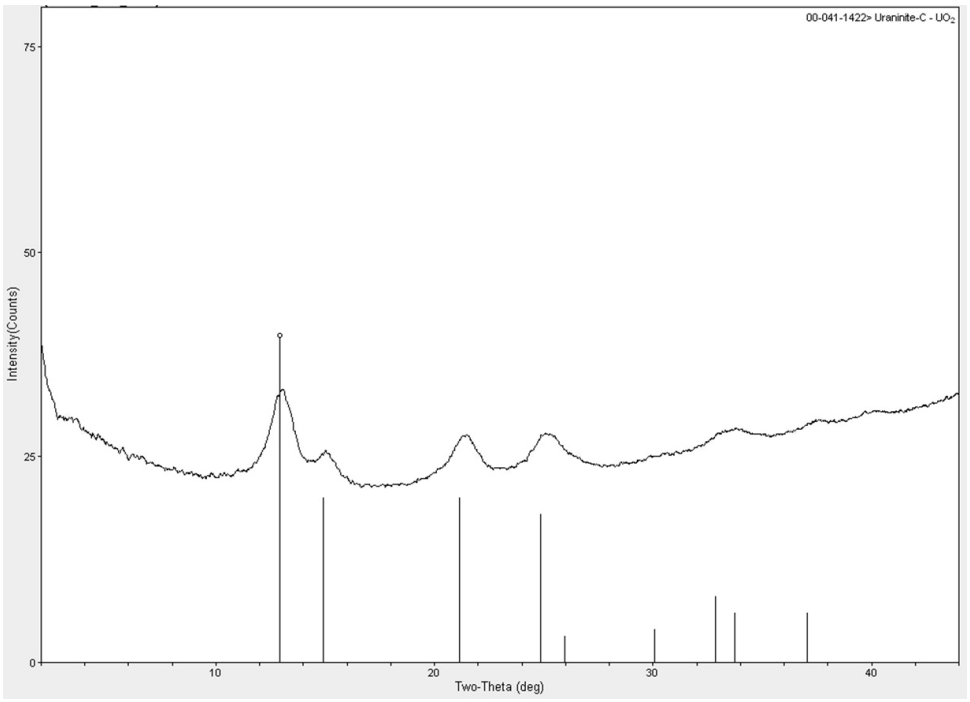

Fig. S2. Uraninite (UO_{2+x}) precipitated in 0.1 M $NaNO_3$ solution containing 100 μM U(VI) and 2 mM $NaHCO_3$ by 1 mM AH_2DS at pH of 6.8 for 1 day. Systematic shift of the peaks toward high angle with respect to reference UO_2 indicates smaller unit cell due to U(VI) in the of the uraninite nano-crystals.

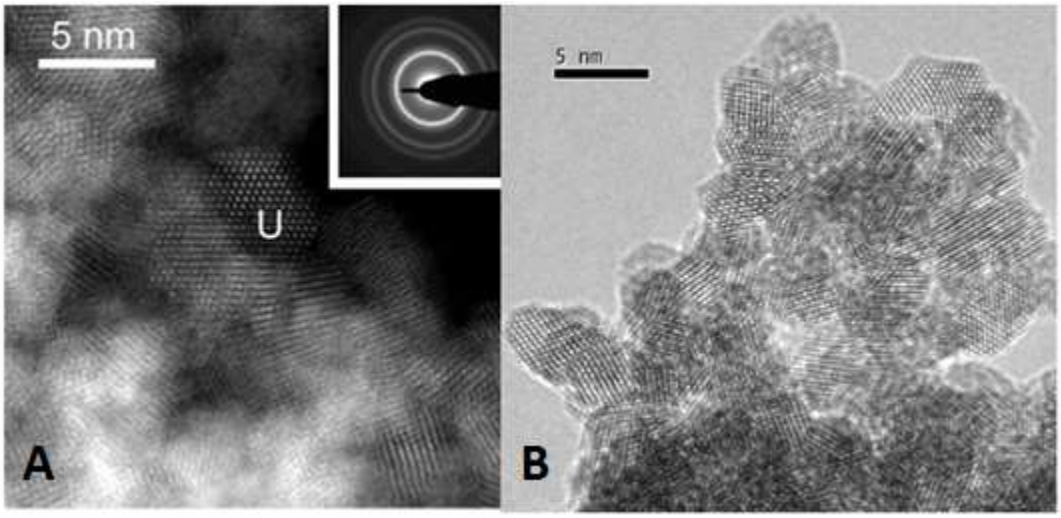

Fig. S3. **A**: Z-contrast image showing an aggregate of uraninite nano-crystals formed during reaction (2 days) of 100 μM U(VI) with 1 mM AH_2DS in 0.1 M $NaNO_3$ containing 2 mM $NaHCO_3$ at pH 6.8. [110]-zone axis of a labeled nano-crystal (U) parallel to the beam direction. Bright spots correspond to U atom positions. Inserted is a selected-area electron diffraction (SAED) pattern of the uraninite nano-crystals; **B**: A high-resolution TEM image showing the uraninite nano-crystals aggregate.

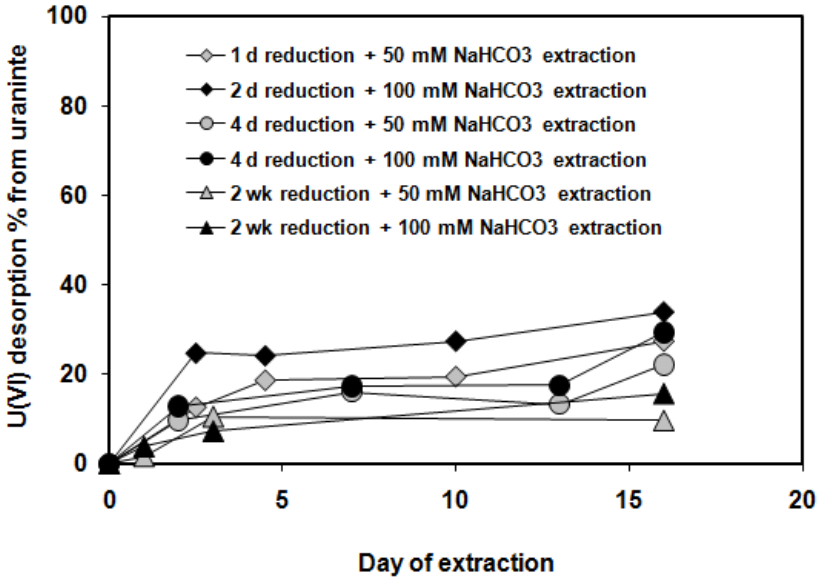

Fig. S4. Percent U(VI) desorption by 50 and 100 mM $NaHCO_3$ for uraninite precipitated by 1 mM AH_2DS in solution of 100 μM U(VI) and 2 mM HCO_3^- at pH 6.8 for 1 day, 4 days, and 2 weeks.

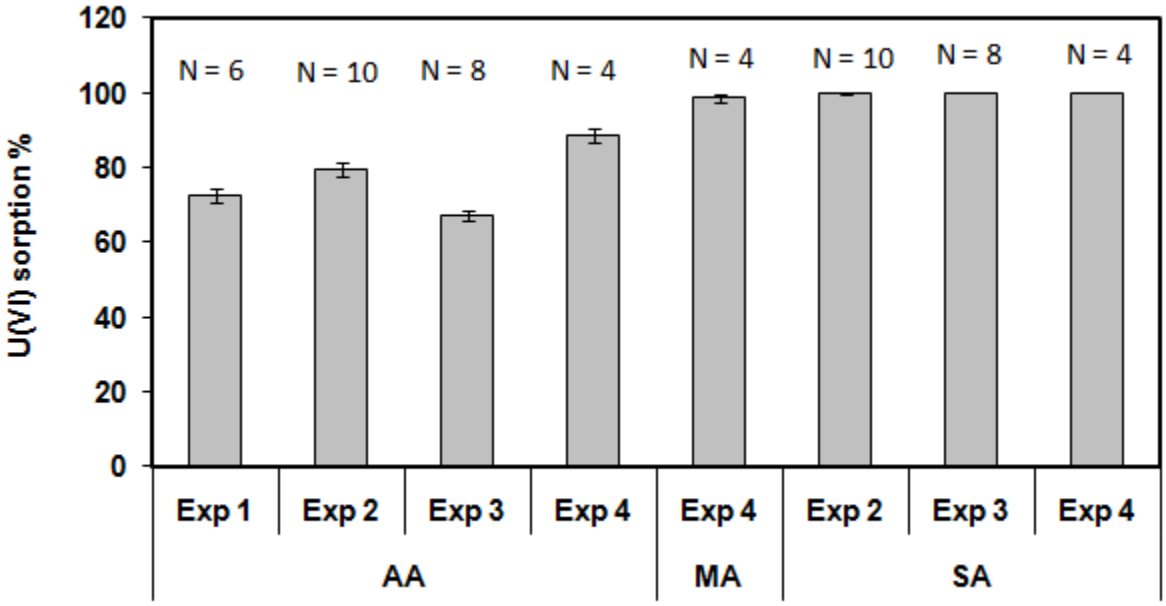

Fig. S5. The percentage of U(VI) sorption to non-nanoporous, mesoporous, and nanoporous aluminum oxides prior to U(VI) reduction and desorption experiments (Fig. 3). See table S1 for detailed experimental condition for sorption experiment 1-4.

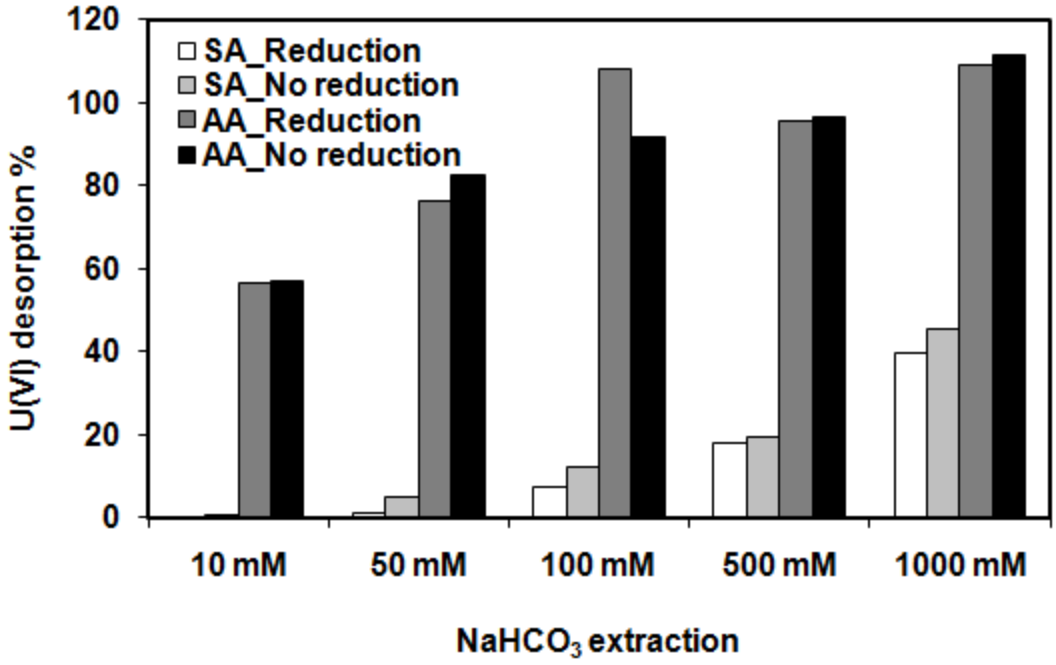

Fig. S6. The percentage of U(VI) desorption by $NaHCO_3$ (10~1000 mM) for 1 week under oxic conditions, immediately after 2-day anoxic bicarbonate extraction from non-nanoporous (AA) and nanoporous (SA) aluminum oxides that were reacted by 1 mM AH_2DS for 1 day. Sorption was conducted by reacting 0.2 g of alumina with 100 μM U(VI) in 2 mM solution at pH of 6.8 for 1 week.

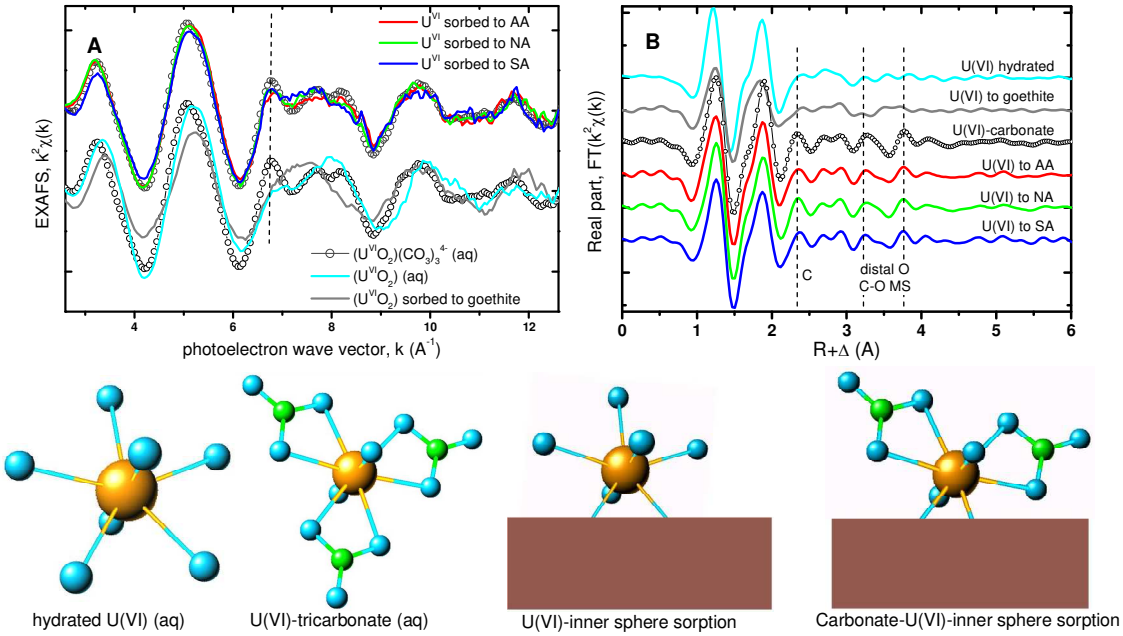

Fig. S7. (A) Top: k^2-weighed EXAFS data from U(VI) sorbed to non-nanoporous, mesoporous, and nanoporous alumina (red, green, blue, respectively) compared to a U(VI)-tricarbonate aqueous standard (symbols). Bottom: Differences in the k^2-weighed EXAFS data between hydrated U(VI) (cyan), a U(VI)-tricarbonate aqueous complex (symbols), and an inner-sphere sorbed U(VI) to geothite (grey). The vertical dashed line indicates a spectral feature characteristic of U(VI)-carbonate binding. (B) Fourier transform of the data in (A) between k=2.6 – 12.2 $Å^{-1}$. Vertical dashed lines indicate the areas of spectral contribution from the C and distal O atoms (shell-by-shell fits are shown on Fig. S7). Molecular models of the aqueous and sorbed complexes are shown below the data.

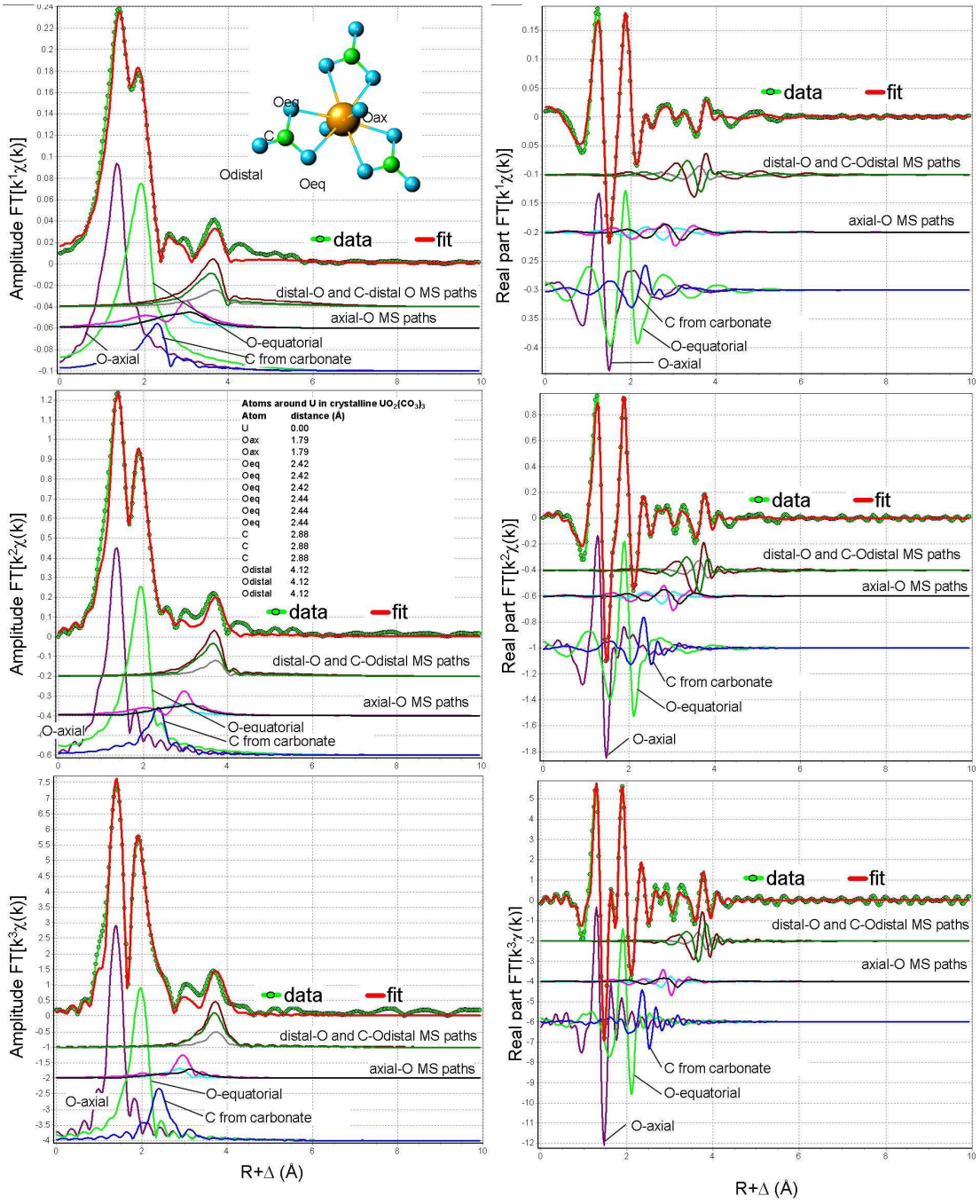

Fig. S8. Amplitude (left) and real part (right) of Fourier transformed k^n-weighed EXAFS data and fit (n=1,2,3 from top to bottom) for the U(VI) tri-carbonate aqueous standard. The data were fit simultaneously at all three k-weights and the best fit parameters are listed in Table S2. Fourier transform range is k= 2.6 – 13.2 $Å^{-1}$ with a 1 $Å^{-1}$ Hanning window and fit range is R=1.2 – 4.0 Å. The contributions from the different shells in the fit are presented offset vertically below the data and overall fit lines.

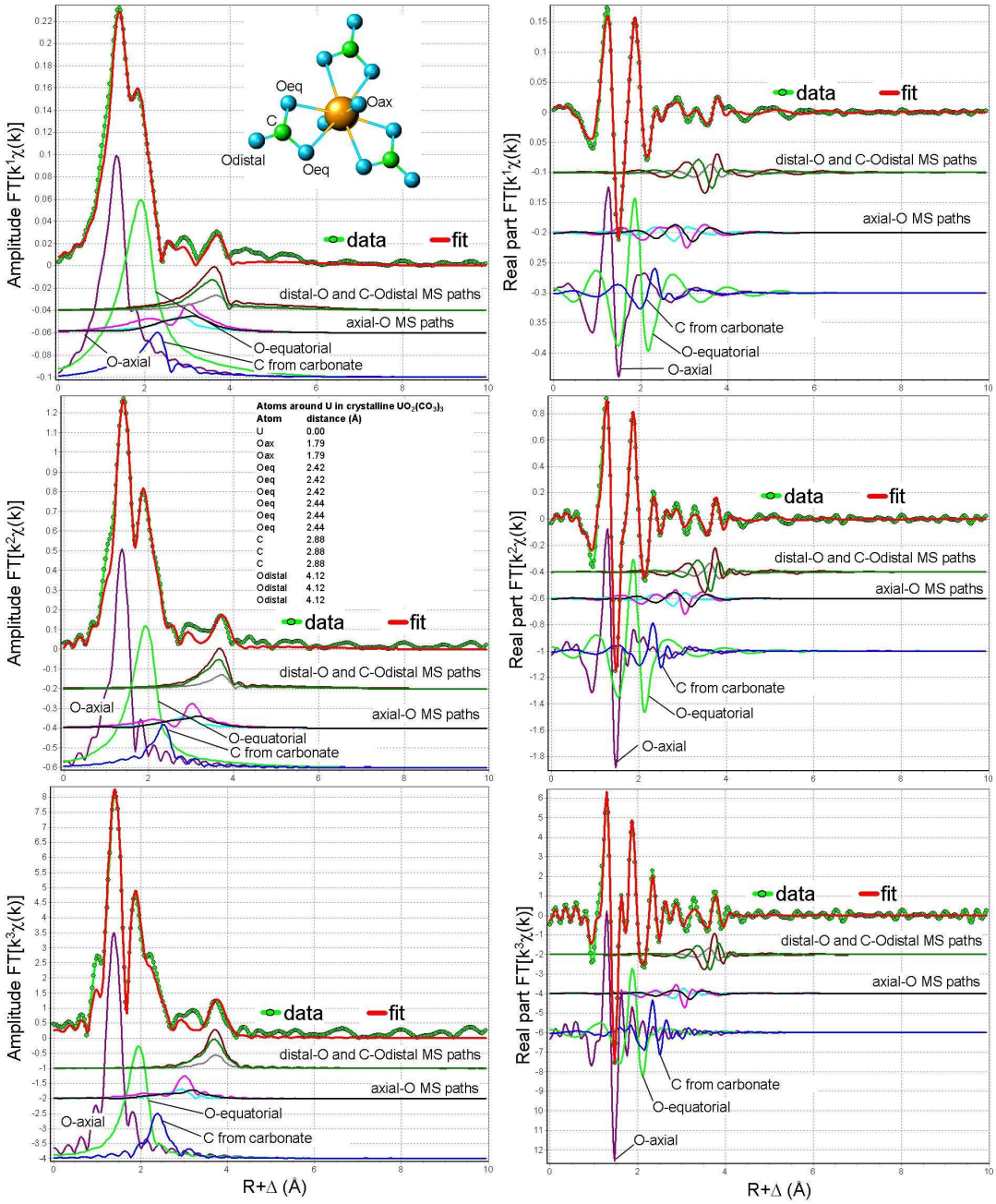

Fig. S9. Amplitude (left) and real part (right) of Fourier transformed k^n-weighed EXAFS data and fit (n=1,2,3 from top to bottom) for the U(VI) adsorbed on alumina sample. The data were fit simultaneously at all three k-weights and the best fit parameters are listed in Table S2. Fourier transform range is k= 2.6 – 13.2 $Å^{-1}$ with a 1 $Å^{-1}$ Hanning window and fit range is R=1.2 – 4.0 Å. The contributions from the different shells in the fit are presented offset vertically below the data and overall fit lines.

Table S1. Detailed experimental setup for 4 sets of U(VI) sorption experiments before reduction by AH_2DS.

	Exp 1	Exp 2	Exp 3	Exp 4
Duration	5 d	7 d	3 d	9 d
U(VI)	100 uM	100 uM	150 uM	100 uM
NaHCO3	2 mM	2 mM	4 mM	2 mM
NaNO3	0.1 M	0.1 M	0.1 M	0.1 M
pH	6.8	6.8	6.8	6.8
Alumina mass	0.2 g	0.2 g	0.45 g	0.16 g
Solution volume	10 mL	10 mL	10 mL	8 mL

Table S2. Refined parameters in the EXAFS fits.

Path[a]	N[b]	R(Å)[c]	σ²(Å²)[d]	ΔE(eV)[e]	DF[f]	R-factor[g]	χ_ν^2 [h]
A) U(VI)-carbonate standard fit with N fixed to the tri-carbonate complex values							
U-Oax	2.0	1.81 ± 0.01	0.0017 ± 0.0004	2.4 ± 0.2	9	0.008	226
U-Oeq	6.0	2.43 ± 0.01	0.0067 ± 0.0006	-0.5			
U-C	3.0	2.88 ± 0.01	0.0020 ± 0.0015	-5.6			
U-Oax1-Oax2	Oax	3.53 ± 0.03	0.0000 ± 0.0043	-3.9			
U-Oax1-U-Oax1	Oax	3.53 ± 0.03	0.0000 ± 0.0043	-3.9			
U-Oax1-U-Oax2	Oax	3.53 ± 0.03	0.0000 ± 0.0043	-3.9			
U-Odistal	C	4.20 ± 0.02	0.0060 ± 0.0019	4.7			
U-Odistal-C	2×C	4.20 ± 0.02	0.0060 ± 0.0019	4.7			
U-C-Odistal-C	C	4.20 ± 0.02	0.0060 ± 0.0019	4.7			
B) Alumina-sorbed U(VI) fit with N fixed to the tri-carbonate complex values							
U-Oax	2.0	1.81 ± 0.01	0.0011 ± 0.0004	3.1 ± 1.1	9	0.011	68
U-Oeq	6.0	2.43 ± 0.01	0.0097 ± 0.0009	0.3			
U-C	3.0	2.88 ± 0.01	0.0030 ± 0.0019	-4.9			
U-Oax1-Oax2	Oax	3.55 ± 0.03	0.0000 ± 0.0038	-3.1			
U-Oax1-U-Oax1	Oax	3.55 ± 0.03	0.0000 ± 0.0038	-3.1			
U-Oax1-U-Oax2	Oax	3.55 ± 0.03	0.0000 ± 0.0038	-3.1			
U-Odistal	C	4.21 ± 0.02	0.0084 ± 0.0027	5.5			
U-Odistal-C	2×C	4.21 ± 0.02	0.0084 ± 0.0027	5.5			
U-C-Odistal-C	C	4.21 ± 0.02	0.0084 ± 0.0027	5.5			
C) U(VI)-carbonate standard fit with Oeq and C coordination numbers refined							
U-Oax	2.0	1.81 ± 0.01	0.0016 ± 0.0005	2.5 ± 0.1	7	0.008	495
U-Oeq	6.0 ± 0.7	2.43 ± 0.01	0.0067 ± 0.0016	-0.4			
U-C	3.2 ± 1.0	2.88 ± 0.01	0.0026 ± 0.0028	-5.5			
U-Oax1-Oax2	Oax	3.54 ± 0.01	0.0000 ± 0.0054	-3.8			
U-Oax1-U-Oax1	Oax	3.54 ± 0.01	0.0000 ± 0.0054	-3.8			
U-Oax1-U-Oax2	Oax	3.54 ± 0.01	0.0000 ± 0.0054	-3.8			
U-Odistal	C	4.21 ± 0.02	0.0067 ± 0.0037	4.8			
U-Odistal-C	2×C	4.21 ± 0.02	0.0067 ± 0.0037	4.8			
U-C-Odistal-C	C	4.21 ± 0.02	0.0067 ± 0.0037	4.8			
D) Alumina-sorbed U(VI) fit with Oeq and C coordination numbers refined							
U-Oax	2.0	1.81 ± 0.01	0.0011 ± 0.0005	3.2 ± 1.3	7	0.011	86
U-Oeq	5.9 ± 1.0	2.43 ± 0.02	0.0096 ± 0.0025	0.3			
U-C	2.9 ± 1.2	2.88 ± 0.02	0.0029 ± 0.0036	-4.8			
U-Oax1-Oax2	Oax	3.55 ± 0.02	0.0000 ± 0.0053	-3.1			
U-Oax1-U-Oax1	Oax	3.55 ± 0.02	0.0000 ± 0.0053	-3.1			
U-Oax1-U-Oax2	Oax	3.55 ± 0.02	0.0000 ± 0.0053	-3.1			
U-Odistal	C	4.21 ± 0.03	0.0083 ± 0.0053	5.6			
U-Odistal-C	2×C	4.21 ± 0.03	0.0083 ± 0.0053	5.6			
U-C-Odistal-C	C	4.21 ± 0.03	0.0083 ± 0.0053	5.6			
E) U(VI)-carbonate standard fit with sigma2 fixed to fits in A)							
U-Oax	2.0	1.81 ± 0.01	0.0016 ± 0.0004	2.4 ± 0.1	10	0.008	359
U-Oeq	6.0 ± 0.3	2.43 ± 0.01	0.0067	-0.4			
U-C	3.1 ± 0.4	2.88 ± 0.01	0.0020	-5.6			
U-Oax1-Oax2	Oax	3.54 ± 0.03	0.0000 ± 0.0017	-3.9			
U-Oax1-U-Oax1	Oax	3.54 ± 0.03	0.0000 ± 0.0017	-3.9			
U-Oax1-U-Oax2	Oax	3.54 ± 0.03	0.0000 ± 0.0017	-3.9			
U-Odistal	C	4.21 ± 0.02	0.0060	4.8			
U-Odistal-C	2×C	4.21 ± 0.02	0.0060	4.8			
U-C-Odistal-C	C	4.21 ± 0.02	0.0060	4.8			
F) Alumina-sorbed U(VI) fit with sigma2 fixed to fits in A)							
U-Oax	2.0	1.81 ± 0.01	0.0011 ± 0.0005	3.3 ± 0.8	10	0.017	84
U-Oeq	5.0 ± 0.3	2.43 ± 0.01	0.0067	0.5			
U-C	2.4 ± 0.4	2.88 ± 0.02	0.0020	-4.7			
U-Oax1-Oax2	Oax	3.56 ± 0.03	0.0000 ± 0.0024	-2.9			
U-Oax1-U-Oax1	Oax	3.56 ± 0.03	0.0000 ± 0.0024	-2.9			
U-Oax1-U-Oax2	Oax	3.56 ± 0.03	0.0000 ± 0.0024	-2.9			
U-Odistal	C	4.21 ± 0.02	0.0060	5.7			
U-Odistal-C	2×C	4.21 ± 0.02	0.0060	5.7			
U-C-Odistal-C	C	4.21 ± 0.02	0.0060	5.7			

(see footnotes and explanations on next page)

a) Photoelectron scattering paths in the EXAFS model used to fit the data. Single-scattering (SS) paths (e.g. U-Oax) correspond to atomic shells; multiple-scattering (MS) paths (e.g. U-Odistal-C) take into account some of the stronger multiple reflections of the photoelectron from neighboring atoms.
b) Coordination number for SS paths or path degeneracy for MS paths. When uncertainties are not given the parameter is held fixed to the shown value during the fit. N of the axial O path is always fixed to 2. MS paths are parametrized as shown relative to the SS paths (e.g. N for path U-Oax1-Oax2 is held to the same value as the U-Oax path, N for path U-Odistal-C is held fixed to twice that for the U-C shell.
c) Radial distance of the atomic shell from U for SS paths or path half-length for MS paths. The change in length for each group of MS paths (Oax and Odistal) was constrained to be the same for all three paths in each group.
d) Debye-Waller factor for the corresponding path. When uncertainties are not given the parameter is held fixed during the fit to the shown value. MS paths corresponding to the Oax shell are grouped together with the same σ^2 variable, MS paths corresponding to the distal O shell are also grouped together with the same σ^2 variable.
e) Energy origin shift parameter, used to account for differences between the experimental and the calculated Fermi level by FEFF. More information on this parameter is given in the FEFF and FEFFIT documentation. The ΔE values for all paths used in the EXAFS model were treated as unknown from the theoretical EXAFS calculation and were calibrated by fitting the U(VI) tri-carbonate standard with the known coordination numbers in this standard (fit A). The *differences* in ΔE values between all paths was then fixed in the EXAFS model, and a single relative ΔE variable for all paths was introduced to account for possible differences in the choice of edge energy between the samples and standard. The listed ΔE values for each path correspond to the absolute differences between the FEFF calculation and the value used in the fit; the uncertainty given is for the overall relative ΔE variable used for all paths.
f) DF=Degrees of Freedom in the fit, the difference between the number of independent data points and the number of parameters used to fit the data. More information on this metric of the fit is given in the FEFFIT documentation.
g) R-factor is a measure of the closeness between the data points and the fit line, without accounting for the number of variables in the model. More information on this metric of the fit is given in the FEFFIT documentation.
h) The reduced-χ^2 parameter accounts for both the differences between the data points and the fit line, and the degrees of freedom in the fit. More information on this metric of the fit is given in the FEFFIT documentation.

Analysis of the EXAFS fits and fit parameters in Table S2

Fit A) is an EXAFS theory calibration fit, in which the Oax, Oeq, and C coordination numbers are held fixed to values for the tri-carbonate U(VI) complex expected to be predominant under the pH 11 conditions and the 1:50 ratio of U(VI):carbonate in this solution standard. The good

reproduction of the data (Fig. S7) demonstrates that the EXAFS model and calculations can reproduce a known U(VI) coordination environment, and calibrates the ΔE parameters for all paths. Fit B) uses the U(VI)-tricarbonate model (fixed coordination numbers) to fit U(VI) sorbed on alumina. The increased values of the σ^2 parameters for the Oeq, C, and Odistal shells relative to fit A) suggest that the smaller FT amplitude in Fig. 5A can be explained by increased disorder in these shells relative to the aqueous standard, likely due to distortions resulting from the sorption process. Fits C) and D) confirm this observation, by relaxing the constraint on the Oeq and C coordination numbers. The Oeq and C numbers minimize to very similar values in the aqueous standard and the alumina sorbed U(VI) samples; the increase in σ^2 parameters between fits C) and D) in this unconstrained fit suggests again that distortion in the shells can explain the reduced FT amplitudes. Fits E) and F) show an attempt to fit the sorbed U(VI) spectrum with σ^2 parameters of the shells constrained to those obtained in fits of the U(VI) carbonate standard. The decreased FT amplitude is modeled in this case by decreased Oeq and C coordination numbers, but the fit quality is lower (R-factor increased to 0.017 from 0.011) indicating better reproduction of the data in fits B) and D) of the sorbed U(VI) spectrum. Thus, the most likely sorption mechanism of U(VI) to alumina surfaces is the outer-sphere adsorption of a distorted U(VI)-tri-carbonate complex.